Della Bella *et al. BMC Methods* (2026) 3:15
https://doi.org/10.1186/s44330-026-00070-x

BMC Methods

METHODOLOGY Open Access

Control of human mesenchymal stromal cell gene expression levels by sound-guided assembly and stimulation

Elena Della Bella[1], Farah Daou[2], Alessandro Cianciosi[1], Junxuan Ma[1], Riccardo Tognato[1], Mauro Alini[1], Andrea Cochis[2], Lia Rimondini[2], Martin J Stoddart[1,4] and Tiziano Serra[1,3*]

Abstract

Background Acoustic fields enable contactless manipulation of cells and multicellular assemblies, offering unique opportunities for three-dimensional (3D) cell culture and mechanobiology. However, standardized and reproducible methodologies that combine sound-guided cell assembly with controlled acoustic stimulation and downstream molecular analysis are still lacking.

Methods We developed a reproducible workflow integrating sound-guided assembly and acoustic stimulation of human bone marrow–derived mesenchymal stromal cell (hBMSC) spheroids within 3D fibrin hydrogels. Using a sound-induced morphogenesis (SIM) platform, spheroids were rapidly organized into circular patterns through low-frequency acoustic. Pattern geometry and stability were quantitatively assessed by image-based radial profile analysis. To evaluate biological responsiveness to assembly and stimulation, spheroids were analyzed under three conditions (randomly dispersed, sound-assembled, and sound-assembled with daily acoustic stimulation) followed by transcriptomic profiling using RNA sequencing and validation by RT-qPCR.

Results Sound-guided assembly consistently generated stable, high-density annular spheroid patterns that were maintained over culture duration and unaffected by subsequent acoustic stimulation. Transcriptomic analysis revealed reproducible changes in gene expression associated with cell–cell interactions, stress regulation, and mechanosensing in assembled spheroids compared with dispersed controls. Additional acoustic stimulation induced a distinct transcriptional signature involving genes related to matrix remodeling and mechanotransduction, confirming biological sensitivity to applied mechanical cues.

Conclusions This method provides a standardized, non-invasive approach to couple spatial cell organization with controlled mechanical stimulation in 3D culture systems. The workflow is compatible with conventional cell culture practices, adaptable to other cell types and hydrogels, and suitable for mechanistic studies investigating how physical cues regulate cellular gene expression. It offers a transferable methodological framework for mechanobiology research and engineered tissue model development.

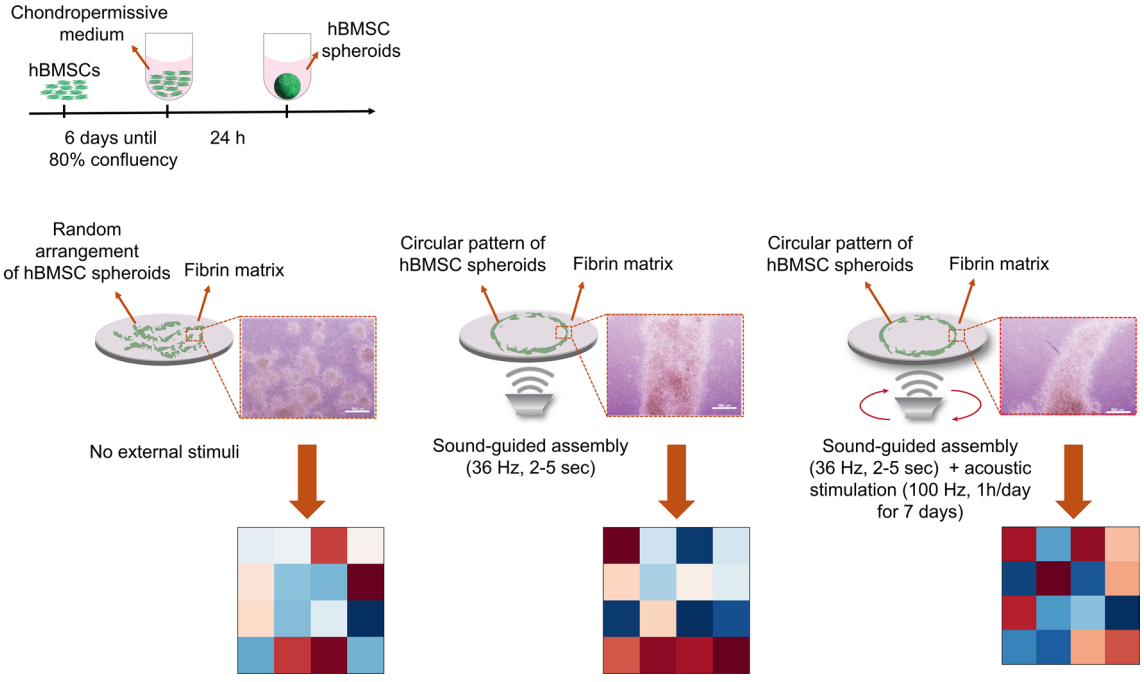
*Correspondence:
Tiziano Serra
tiziano.serra@aofoundation.org

Full list of author information is available at the end of the article

© The Author(s) 2026. **Open Access** This article is licensed under a Creative Commons Attribution-NonCommercial-NoDerivatives 4.0 International License, which permits any non-commercial use, sharing, distribution and reproduction in any medium or format, as long as you give appropriate credit to the original author(s) and the source, provide a link to the Creative Commons licence, and indicate if you modified the licensed material. You do not have permission under this licence to share adapted material derived from this article or parts of it. The images or other third party material in this article are included in the article's Creative Commons licence, unless indicated otherwise in a credit line to the material. If material is not included in the article's Creative Commons licence and your intended use is not permitted by statutory regulation or exceeds the permitted use, you will need to obtain permission directly from the copyright holder. To view a copy of this licence, visit http://creativecommons.org/licenses/by-nc-nd/4.0/.

Keywords Bio-assembly, Sound-guided assembly, Acoustic stimulation, Gene expression, RNA sequencing, MSCs, Condensation

Graphical Abstract



Introduction

Human bone marrow-derived mesenchymal stromal cells (hBMSCs) possess the remarkable ability to differentiate into a variety of cell types, placing them at the forefront of regenerative medicine and tissue engineering [1, 2]. Understanding and controlling the behavior of hBMSCs—particularly their differentiation, proliferation, and gene expression—is essential for developing effective therapeutic strategies. While mechanical and biochemical cues have traditionally been explored to guide stem cell fate, the complex interplay of these factors in three-dimensional (3D) microenvironments remains a critical area of investigation [3, 4].

Among emerging bioengineering strategies, acoustic stimulation has gained increasing attention as a non-invasive, contactless method to modulate cellular behavior. By applying mechanical forces through sound waves, this technique has been shown to influence several biological processes including migration, alignment, and differentiation of various cell types [5, 6]. In hBMSCs, low-frequency acoustic stimulation has been associated with enhanced expression of osteogenic and chondrogenic markers, suggesting its utility in musculoskeletal tissue engineering [7].

Beyond modulation of gene expression, acoustic fields can be harnessed to spatially organize cells and cellular aggregates, a concept often referred to as sound-guided assembly or acoustic patterning. Through phenomena such as standing acoustic waves, cells can be rapidly and reproducibly organized into well-defined 2D and 3D patterns within hydrogels or microfluidic environments [8]. These patterns include rings, lines, and clusters, allowing precise control over local cell density and spatial distribution, which are known to critically affect stem cell behavior.

Several studies have demonstrated the power of acoustic tweezers and surface acoustic wave (SAW)-based platforms for cellular assembly. For instance, Guo et al. used SAW fields to control intercellular distances and cell–cell interactions in a highly tunable manner [9]. Armstrong et al. showed that acoustic patterning of myoblasts in collagen-based hydrogels enabled the fabrication of aligned muscle tissue with improved structural and functional properties [10]. Furthermore, Ozcelik et al. provided a comprehensive overview of how acoustic tweezers can be used to manipulate single cells and multicellular aggregates, underlining their versatility and biocompatibility for life science applications [11].

Despite these advances, the biological consequences of acoustic assembly on gene expression remain largely unexplored. Little is known about how the local density enhancement achieved through acoustic patterning affects the transcriptomic landscape of stem cells within 3D environments. Also, there is a lack of standardized

methods that combine acoustic assembly with subsequent stimulation and document the resulting biological effects.

In this work, we describe a method for sound-guided assembly of hBMSC spheroids in a 3D fibrin hydrogel and examine how this spatial organization affects gene expression compared to randomly distributed spheroids. We further explore the impact of continued short-term acoustic stimulation following initial patterning. By integrating acoustic physics with stem cell biology, this work provides new insights into how physical forces and spatial organization can be leveraged to influence stem cell phenotype in engineered tissue environments.

Previously, we demonstrated that sound-guided patterning can be used to spatially organize endothelial cells and pericytes, leading to the formation of continuous capillary-like structures through increased local cell density and mechanical condensation. This was accompanied by significant molecular remodeling, with over 900 proteins differentially regulated and VEGF-A identified as a key upstream regulator driving angiogenic pathways [12].

In a parallel study, we employed a similar contactless assembly strategy to create a physiologically relevant in vitro model of annulus fibrosus innervation using spatially organized dorsal root ganglia tissue units. The spatial proximity between tissues was shown to be critical for multi-level functional crosstalk and axon guidance, underlining the importance of recapitulating anatomical architecture when engineering multicellular systems [13].

Building upon these findings, the present study investigates how acoustic assembly and stimulation influence the transcriptomic landscape of hBMSCs in 3D.

Materials and methods

hBMSCs spheroids fabrication

The study was conducted in accordance with the Declaration of Helsinki. hBMSCs were previously obtained from a 58-years old male donor, undergoing spinal surgery at the Freiburg University Hospital, Germany, with written informed consent and full ethical approval (Ethik-Kommission der Albert-Ludwigs-Universität Freiburg, EK-326/08). Cells were isolated and cryopreserved as described before [14, 15]. For this study, cells were thawed and expanded in alpha Minimum Essential Medium (αMEM; Gibco, Thermo Fisher, Zürich, Switzerland) with 10% fetal bovine serum (FBS; Corning, Corning, NY, USA), 100 U/mL penicillin, 100 µg/mL streptomycin (Gibco, Thermo Fisher) and 5 ng/mL recombinant human basic fibroblast growth factor (bFGF, Fitzgerald Industries International, Acton, MA, USA). The cells were detached when 80% confluent with 0.05% Trypsin/EDTA (Gibco, Thermo Fisher), counted, and resuspended in chondropermissive medium. The chondropermissive medium included Dulbecco's Modified Eagle Medium (DMEM) with 4.5 g/L glucose (Gibco, Thermo Fisher), 0.11 g/L sodium pyruvate (Sigma-Aldrich, Buchs, Switzerland), Corning ITS+ Premix (a pre-made mix of 6.25 µg/ml human recombinant insulin, 6.25 µg/ml human natural transferrin, 6.25 µg/ml selenious acid, 1.25 mg/ml bovine serum albumin, 5.35 µg/ml linoleic acid), 1% non-essential amino acids (Gibco, Thermo Fisher), 50 µg/mL L-ascorbic acid 2-phosphate sesquimagnesium salt hydrate (Sigma-Aldrich), 100 nM dexamethasone (Sigma-Aldrich), 100 µg/mL streptomycin, 100 U/mL penicillin (Gibco, Thermo Fisher). hBMSCs spheroids were fabricated using the AggreWell™ 400 (STEMCELL Technologies, Vancouver, Canada). For each well, 1.8×10^6 cells in 5 mL culture medium were seeded per well to generate around 7000 spheroids, containing initially approximately 260 cells. The spheroids were cultured for 24 h before using them for further experiments.

Rheological characterization of fibrin

Rheological properties the fibrin were characterized using an Anton Paar MCR 702 rheometer (Anton Paar, Graz, Austria) with a 25 mm parallel plate geometry at a 500 µm gap. A solvent trap was used to limit evaporation phenomenon during the experiments. All measurements were conducted by loading the freshly prepared hydrogel precursors on the lower plate at room temperature (25 °C). The oscillatory measurements were performed with 5% strain and 1 rad $s-1$ angular frequency, these values were selected from the LVR.

Sound-guided assembly of hBMSCs spheroids into a fibrin matrix

Approximately 2.8×10^4 spheroids were collected from four wells. After centrifuging at 400 g for 5 min at room temperature, the pellets were resuspended in chondropermissive medium and kept on ice until use. Immediately before assembly, the spheroid suspension was mixed with thrombin from human plasma, ε-aminocaproic acid, and fibrinogen from human plasma (all from Sigma-Aldrich) to a final concentration of 5.833×10^3 spheroids/mL, 0.333 U/mL, 5 nM, and 2.5 mg/mL, respectively.

Once mixed, a volume of 0.3 mL/sample was immediately used to assemble the spheroids in circular patterns (~1750 spheroids/sample). All procedures were conducted under sterile conditions within a Class II biosafety cabinet. The SIM device was disinfected with 70% ethanol before each use, and the acoustic stimulation was applied through the closed Petri dish lid to maintain sterility and prevent any direct contact with the culture medium. The assembly process was performed in a circular-shaped frame with a diameter of 14.9 mm and a depth of 1 mm. The frame inserts were constructed using

poly(methyl methacrylate) (PMMA) sheets to fit in 6-mm petri dishes and fixed using medical-grade double-sided adhesive tape (3 M, St. Paul, MN, USA). Care was taken to ensure an even coverage of liquid on the frame and to avoid bubbles. A specialized system, referred to as Sound Induced Morphogenesis (SIM) device (CymatiX, mimiX Biotherapeutics, Biel/Bienne, Switzerland) [16, 17], was utilized for sound-guided assembly of spheroids, facilitating their spatial organization into circles. The circular pattern was created by stimulating the spheroid solution at 36 Hz for 2–5 s. The amplitude of vibration was manually adjusted to ensure circular liquid surface template. The whole patterning process was performed in ice-cold condition to prevent premature fibrin formation. The constructs were then carefully incubated at 37 °C to allow fibrinogen cleavage by thrombin. After fibrin formation, four mL of chondropermissive medium was added to each sample. The effect of condensation in assembled samples ("A") was compared to samples with randomly dispersed spheroids ("D"). Moreover, assembled spheroids were subjected to additional acoustic stimulation ("A + S") with acoustic waves at 100 Hz, one hour per day with a continuous cycle. Four replicates were included in each group. The culture was performed in chondropermissive medium and lasted for 7 consecutive days. Medium change was performed every 48 h, and on each of these occasions, acoustic stimulation was applied immediately afterward.

Construct characterization

The constructs were fixed using 4% neutral buffered formalin (Formafix, Hittnau, Switzerland) for 1 h at room temperature. The actin cytoskeleton was stained with F-Actin Phalloidin Conjugates Alexa 488 (ReadyProbes™ Reagent, Thermo Fisher) according to the manufacturer's protocol and nuclei were stained using 2 µM Hoechst (Sigma-Aldrich). The staining was performed at room temperature for 1 h. Transmitted light imaging was performed using EVOS™ FL Auto 2 Imaging System (Thermo Fisher) at 4× magnification. Background of images were corrected using the BASIC plugin [18] in Fiji/ImageJ v.1.54f (NIH, Bethesda, MD, USA). The corrected images were stitched using "Grid/collection stitching" function in Fiji/ImageJ.

The fluorescent imaging was performed using an LSM-800 confocal microscope (Carl Zeiss, Oberkochen, Germany) at 5× magnification. Excitation wavelength was 488 nm and 405 for F-Actin Phalloidin and Hoechst staining, respectively. Their detection wavelengths were set as 400 ~ 650 nm and 400 ~ 600 nm wavelengths, respectively. The pixel size was 0.624 µm × 0.624 µm. The pin hole was set 460 µm. For patterned structure, a "z-stack" imaging was performed when necessary to cover the whole range of the structure in z direction.

Radial profile analysis

The geometry and reproducibility of the hBMSCs spheroids patterns were measured from the images acquired for the three different conditions: "A", "D", and "A+S". An ImageJ macro was created to extract the morphological characteristics of the pattern. The ImageJ's plugin "Radial profile" was used to measure diameter and thickness of the microcapillary ring. Briefly, the ImageJ's plugin measured the intensity values along the radius of a region of interest (ROI) placed concentrically with the pattern, the radius was spun over 360 degrees and the intensity values were integrated and plotted against the radial distance from the center of the ROI. A total of 4 images per experimental group were analyzed and the results plotted in the corresponding graph.

RNA isolation, quantity and quality assessment

Total RNA was extracted using TRIreagent (Molecular Research Center Inc., Cincinnati, OH, USA) following the manufacturer's protocol. The RNA was then purified using the Qiagen RNeasy Mini Kit (Qiagen, Hilden, Germany) as per the manufacturer's instructions. RNA yield and quality were preliminarily evaluated using a NanoDrop One UV-Vis spectrophotometer (Thermo Fisher). Total RNA concentration was determined using the Qubit™ RNA BR Assay Kit and Qubit™ 4.0 Fluorometer (Invitrogen, Thermo Fisher), whereas RNA integrity was assessed using the Agilent 4200 TapeStation System (G2991AA) with the Agilent High Sensitivity RNA ScreenTape Assay (Agilent Technologies Inc., Santa Clara, CA, USA). All RNA samples exhibited an RNA integrity number (RIN) ≥ 9, indicating high quality.

RNA-seq library preparation

For RNA-seq library preparation, 300 ng of total RNA per sample were subjected to a ribosomal RNA depletion using the Illumina™ Stranded Total RNA Prep, Ligation with Ribo-Zero™ Plus Kit (Illumina, San Diego, CA, USA). The resulting libraries were quantified using Qubit™ 1X dsDNA HS Assay Kit and Qubit™ 4.0 Fluorometer (Invitrogen, Thermo Fisher Scientific) and assessed for quality using Agilent 4200 TapeStation System and Agilent High Sensitivity D1000 ScreenTape Assay (Agilent Technologies Inc.). Finally, the libraries were sequenced on the Illumina NextSeq™ 550 platform (Illumina) using a NextSeq 500/550 High Output Kit v2.5 (150 cycles, 2 × 75 bp read length, paired end) (Illumina).

RNA-seq bioinformatics

For RNA-Seq bioinformatics, we followed a protocol similar to the one previously described by Daou et al. [19]. Briefly, FastQC [20] and MultiQC [21] software were used to verify the quality of RNA-seq data. Subsequently, the RSEM computational pipeline [22] was used

to quantify the levels of expression of each human gene annotated to Ensembl v100 database [23], using hg38 as reference genome and setting STAR as aligner [24]. We focused our analysis on genes expressed with a TPM > 1 in at least one sample. DESeq2 [25] was used to define differentially expressed genes (DEGs) with the following thresholds: |log2FC| > 0.5 and p.adj < 0.1. Heatmaps showing unsupervised hierarchical clustering of genes were produced using the "pheatmap" function in package of R. Functions were selected manually based on relevance to the experimental purposes. Volcano plots were produced using ggplot2 library in R [26]. The RNA-Seq data are available in the NCBI GEO.

Gene expression analysis

Quantitative real-time PCR (RT-qPCR) was performed to validate the raw expression levels of 6 genes identified with RNA-seq. One µg of the isolated total RNA was treated with DNase I to remove genomic DNA contamination. Then, reverse transcription was performed using the iScriptTM gDNA Clear cDNA Synthesis Kit (Bio-Rad Laboratories, Milan, Italy) on a Mastercycler X50s thermal cycler (Eppendorf, Milan, Italy). The genes of interest, namely C-X-C Motif Chemokine Ligand 6 (*CXCL6*), C-X-C Motif Chemokine Ligand 8 (*CXCL8*), Integrin Binding Sialoprotein (*IBSP*), Integrin Subunit Alpha 8 (*ITGA8*), Sorting Nexin 22 (*SNX22*), and Superoxide Dismutase 2 (*SOD2*), together with the reference gene glyceraldehyde 3-phosphate dehydrogenase (*GAPDH*), were analyzed via qPCR (Table 1). The reactions used 1 ng/µL of cDNA, SsoAdvanced™ Universal SYBR® Green Supermix (Bio-Rad Laboratories), and primers at a concentration of 2.5 µM. The reactions were performed and monitored using a thermal cycler (CFX96TM Real-Time System, Bio-Rad Laboratories). The cycle threshold for each gene of interest was normalized against the reference gene and results were expressed as $2^{-\Delta Cq}$.

Table 1 Sequences of the primers used for gene expression analysis

Target Genes	Forward Primer sequence	Reverse Primer sequence
CXCL6	5′- CGC TTC TCC CTG AAG TTT AC -3′	5′- TGC CAA AGG GTT CAA TAA CT -3′
CXCL8	5′- GAC AAG AGC CAG GAA GAA AC -3′	5′- CAC ACA GAG CTG CAG AAA T -3′
GAPDH	5′- GTA TGA CAA CAG CCT CAA GAT – 3′	5′- GTC CTT CCA CGA TAC CAA AG -3′
IBSP	5′- CAG AAG AGG AGG AGG AAG AA -3′	5′- CCC AGT GTT GTA GCA GAA AG -3′
ITGA8	5′- CCA GAG AAG TAG GGC AAA TC -3′	5′- CAC TAC CGA ATC TCC CAA AC -3′
SNX22	5′- GCT GGA GGT GGT AGA ATT TG -3′	5′- CCC AAA GTG CTG GGA TTA C -3′
SOD2	5′- GAC AAA CCT CAG CCC TAA C -3′	5′- CCG TCA GCT TCT CCT TAA AC -3′

Statistical analysis

Statistical analysis on RT-qPCR results we performed on GraphPad Prism v.10.1.2 (GraphPad Software LLC, Boston, MA, USA). Normal distribution of data and homoscedasticity were preliminary checked with Shapiro-Wilk's and Levene's test respectively. An ordinary one-way ANOVA followed by a Dunnett's test was performed to compare "D" vs. "A", and "A + S" vs. "A". p values < 0.05 were considered as statistically significant.

Results

Spheroid pattern fabrication and characterization

To ensure compatibility of the fibrinogen-based hydrogel precursor with the acoustic patterning process, we performed a rheological characterization of the hydrogel precursor. An oscillatory analysis has been performed to investigate the material's resistance to flow under dynamic shear conditions. The complex viscosity showed over 5 minutes a constant linear trend with values around 400 mPa·s (Fig. 1A). Furthermore, the time sweep performed on the precursor formulation (Fig. 1B) showed the trends of the elastic (G') and viscous (G") modulus over time (5 min) indicating a very fast sol-to-gel transition confirming the formation of a stable gel, which was further characterized via frequency sweep. These analyses are important to better understand the kinetic of the enzymatic crosslinking reaction and to define the operational window for acoustic patterning. The kinetic of the sound-driven assembly in fibrin and gelatin methacroyl (GelMA) precursors is relatively fast (less than 5 s), as already demonstrated [16, 27].

Together, the rheological characterization and spatial patterning experiments demonstrate that the fibrinogen precursor formulation exhibits both the processability and the gelation kinetics required for successful sound-guided assembly of hBMSC spheroids within fibrin gels.

Figure 1C illustrates the effect of sound-guided assembly on the spatial organization of hBMSC spheroids within fibrin hydrogels. When spheroids were not assembled (dispersed condition, "D"), they exhibited a disordered and diffuse distribution within the hydrogel, as shown by both brightfield and fluorescence imaging, with no defined spatial pattern. In contrast, sound-guided assembly ("A") led to the rapid formation of well-defined ring-shaped structures. This organized spatial pattern was clearly visible in transmitted light after assembly. The samples were fixed on day 7 and cytoskeleton of cells were stained using F-actin Phalloidin Alexa Fluor™ 488. These fluorescent images showed that the cells followed homogeneous alignment in the sound-guided assembly in contrast to the randomized alignment in the Dispersed

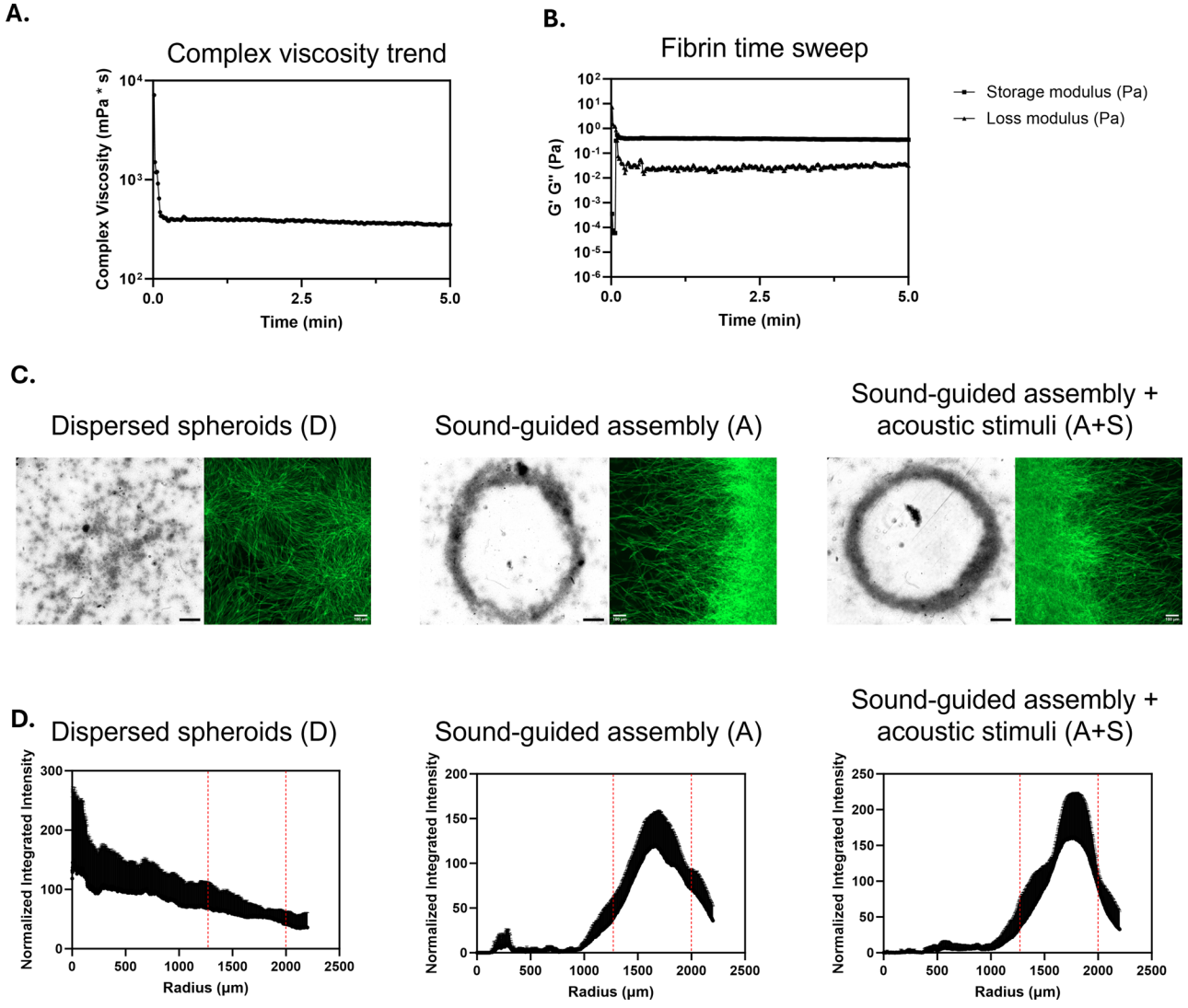


Fig. 1 Qualitative and quantitative assessment of the successful sound-guided assembly approach on the fibrin-based matrix. **A.** Rotational viscosity and **B**. oscillatory time sweep of fibrinogen solution. **(C)** Transmitted light images of the three experimental groups (dispersed spheroids "D", sound-guided assembly "A", and sound-guided assembly with additional acoustic stimulation "A + S") were captured on day 2. Fluorescence images were acquired on day 7 following fixation and staining with F-actin Phalloidin Alexa Fluor™ 488. The scale bars for transmitted light images are 500 μm; the scale bars for fluorescent images are 100 μm. Fluorescence images were consistently taken from the convex side of the rings, where anisotropic cell alignment is highly reproducible. **(D)** Radial profile distribution of the spheroids embedded in the fibrin matrix for the three experimental groups: dispersed spheroids ("D"), sound-guided assembly ("A"), and sound-guided assembly with additional acoustic stimulation ("A + S"). Line thickness refers to ±standard deviation for each single point. Region between dashed red lines refers to the distance from the center where the assembled cells are in the "A" and "A + S" samples, while in "D" the same region it is indicated for comparison

spheroids. Additional acoustic stimulation of the assembled spheroids ("A + S") did not affect cell condensation, as showed by the maintenance of the circular pattern (Fig. 1C, transmitted light images).

Quantitative assessment of spheroid distribution was performed by analyzing the normalized integrated intensity as a function of radial distance from the center of the construct (Fig. 1D). Dispersed spheroids displayed a low and broadly uniform intensity profile, consistent with a scattered particle distribution. In contrast, the assembled spheroids showed a distinct and narrow intensity peak at a defined radial distance, corresponding to the location of the assembled spheroid ring. This peak was maintained in the A + S condition, further confirming the stability of the spheroid organization over time.

Identification of differentially expressed genes

Unsupervised hierarchical clustering of RNAseq results revealed three groups of genes with different expression levels in spheroids that were cultured dispersed ("D"), assembled ("A"), or assembled followed by acoustic stimulation ("A + S", Fig. 2A).

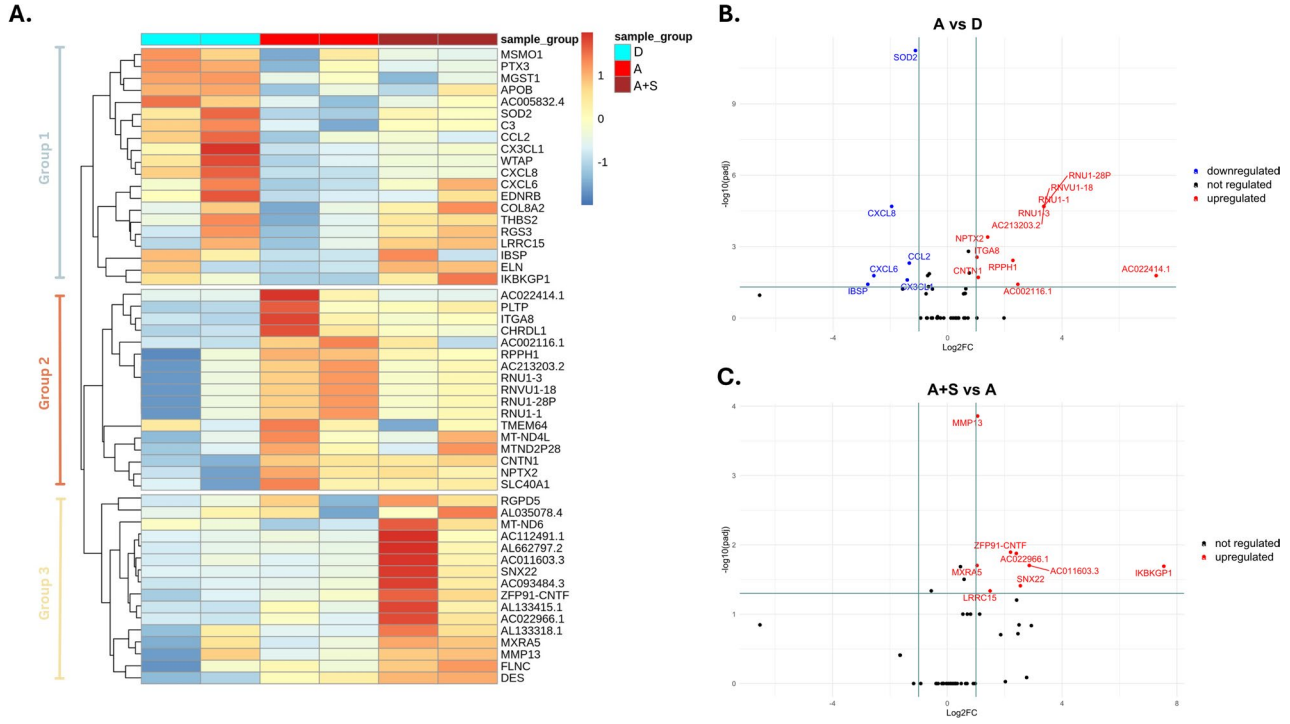


Fig. 2 **A**. Heatmap of gene expression profiles across human bone marrow mesenchymal stromal cells (hBMSCs) dispersed spheroids ("D"), sound-assembled ("A"), and sound-assembled with additional acoustic stimulation ("A + S"). Hierarchical clustering identified three main groups of genes with different expression profiles among culture conditions. Rows represent genes and columns represent samples. Expression levels are color-coded, with red indicating high expression and blue indicating low expression. **B.** Volcano plot of differentially expressed genes between sound-guided assembly of spheroids ("A") vs. dispersed ("D"). **C**. Volcano plot of differentially expressed genes between assembled and acoustically stimulated ("A + S") vs. assembled spheroids ("A"). In volcano plots, each point represents a gene, plotted according to its $\log_2$ fold change (Log2FC, x-axis) and $-\log_{10}$ adjusted p-value (padj, y-axis). Differentially expressed genes (padj < 0.05 and | Log2FC | > 1) are highlighted with different colors: upregulated genes in red and downregulated genes in blue. Non-significant genes are shown in black

In assembled spheroids, 11 genes were upregulated and 6 were downregulated compared to randomly dispersed spheroids (Fig. 2B). Further acoustic stimulation of the assembled spheroids resulted in the upregulation of 8 genes, in comparison to the patterned, but not stimulated spheroids (Fig. 2C). Table 2 reports the $\log_2$ fold changes and adjusted p values for each gene identified with hierarchical clustering.

The expression of *CXCL6*, *CXCL8*, *IBSP*, *SOD2* (Group 1 genes), *ITGA8* (Group 2), and *SNX22* (Group 3) was further analyzed by qPCR to validate RNAseq results. The results confirmed the downregulation of *CXCL6* and *SOD2* in assembled vs. dispersed spheroids (Fig. 3). The expression of these two genes is non-significantly increased again when assembled spheroids are further acoustically stimulated. Similar trends were observed for *CXCL8* and *IBSP*, though the results were not statistically significant.

Discussion

The aim of this study was to identify transcriptomic changes in hBMSC spheroids when cultured in fibrin hydrogels and either randomly dispersed, sound-assembled, and assembled followed by further acoustic stimulation for 1 h/day for 7 days. The fluorescence images shown in Fig. 1C provide morphological confirmation of the effects of sound-guided assembly on hBMSC spheroid organization. In the dispersed condition (D), spheroids appeared randomly distributed within the fibrin matrix and displayed low, diffuse F-Actin signal intensity, indicating limited cytoskeletal organization. In contrast, the sound-assembled constructs (A) formed a compact circular ring with strong F-Actin staining and increased nuclear density, consistent with enhanced cell condensation and actin cytoskeleton alignment. The assembled and stimulated group (A + S) maintained this circular configuration after seven days, demonstrating that the applied acoustic stimulation (100 Hz, 1 h per day) preserved structural integrity without disrupting the pattern. This morphological evidence supports that the sound-guided assembly establishes a localized high-density region promoting intercellular contact and mechanical coupling, which correlates with the transcriptional modulation of stress-, adhesion-, and matrix-related genes observed in the RNAseq data.

Table 2 Log_2 fold change (Log2FC) and adjusted p values (padj) for genes identified with unsupervised hierarchical clustering. Comparisons between assembled (A) vs. dispersed spheroids (D) and assembled stimulated (PS) vs. assembled spheroids (A)

Gene symbol	A vs. D		A + S vs. S	
	Log2FC	padj	Log2FC	padj
AC002116.1	2.456	0.038	-1.173	1.000
AC005832.4	-1.569	0.060	0.642	1.000
AC011603.3	0.385	1.000	2.856	0.020
AC022414.1	7.289	0.017	-6.525	0.143
AC022966.1	0.713	1.000	2.405	0.013
AC093484.3	0.570	1.000	2.463	0.191
AC112491.1	0.320	1.000	2.929	0.146
AC213203.2	3.366	0.000	-1.644	0.390
AL035078.4	0.116	1.000	0.974	1.000
AL133318.1	-0.529	1.000	2.416	0.063
AL133415.1	1.024	1.000	1.860	0.197
AL662797.2	0.382	1.000	2.500	0.143
APOB	-0.666	0.048	0.265	1.000
C3	-0.638	0.014	0.293	1.000
CCL2	-1.338	0.005	0.273	1.000
CHRDL1	0.729	0.002	-0.376	1.000
CNTN1	1.072	0.020	-0.318	1.000
COL8A2	-0.731	1.000	1.128	0.100
CX3CL1	-1.409	0.025	0.485	1.000
CXCL6	-2.575	0.017	2.023	0.940
CXCL8	-1.953	0.000	0.687	1.000
DES	0.618	0.093	0.109	1.000
EDNRB	-0.751	0.096	0.160	1.000
ELN	-0.350	1.000	0.697	0.100
FLNC	0.264	1.000	0.344	1.000
IBSP	-2.786	0.038	2.765	0.818
IKBKGP1	-6.567	0.110	7.545	0.020
ITGA8	1.026	0.003	-0.390	1.000
LRRC15	-0.941	1.000	1.491	0.046
MGST1	-0.349	0.884	-0.188	1.000
MMP13	-0.371	1.000	1.057	0.000
MSMO1	-0.712	1.000	0.033	1.000
MT-ND4L	0.602	0.093	-0.029	1.000
MT-ND6	-0.247	1.000	0.810	0.100
MTND2P28	0.638	0.059	-0.031	1.000
MXRA5	-0.132	1.000	1.036	0.020
NPTX2	1.402	0.000	-0.156	1.000
PLTP	0.561	0.096	-0.130	1.000
PTX3	-0.694	0.016	0.096	1.000
RGPD5	0.612	1.000	0.907	1.000
RGS3	-0.358	1.000	0.544	0.100
RNU1-1	3.366	0.000	-1.644	0.390
RNU1-28P	3.366	0.000	-1.644	0.390
RNU1-3	3.366	0.000	-1.644	0.390
RNVU1-18	3.366	0.000	-1.644	0.390
RPPH1	2.283	0.004	-0.925	1.000
SLC40A1	0.759	0.013	-0.148	1.000
SNX22	n/a	n/a	2.546	0.039
SOD2	-1.123	0.000	0.459	0.021
THBS2	-0.567	1.000	0.585	0.031
TMEM64	0.191	1.000	-0.559	0.046
WTAP	-0.530	0.061	0.206	1.000
ZFP91-CNTF	1.972	1.000	2.203	0.013

RNAseq identified three major groups of genes with different profiles across the groups. Group 1 genes, tendentially more expressed in dispersed spheroids ("D"), included genes involved in inflammatory responses and blood vessel morphogenesis such as *C3*, *CCL2*, *CXCL6*, *CX3CL1*, *CXCL8*, *PTX3*, *SOD2*, *APOB*, *COL8A2*. In particular, the expression of *CXCL6* and *SOD2* was significantly downregulated in assembled spheroids. We hypothesize that these changes in gene expression are directly correlated with local density enhancement. Indeed, the *CXCL6* gene encodes for C-X-C motif chemokine 6, also known as Granulocyte chemotactic protein 2 (GCP-2), a chemokine involved in inflammation, cell migration and proliferation [28]. Overexpressing GCP-2 in adipose derived MSCs in a myocardial infarction model improves their angiogenic and survival properties [29], suggesting that its expression is less required when cell-cell communication is improved in absence of an inflammatory stimulus. Similar considerations can be applied to the expression of *SOD2*, encoding Superoxide Dismutase 2. Indeed, oxidative stress and the formation of stress fibers are reduced when cells reach confluency [30, 31], and the decreased expression of *SOD2* when cells are cultured in a condensed state and not further stimulated might reflect a lower need for scavenging superoxide anion radicals. *SOD2* expression can be induced by the activity of several transcriptions factors, such as AP-1, AP-2, CCAAT-enhancer-binding protein (C/EBP) and Sp1 [32] that can be also downregulated or inhibited when cells reach high confluency [33–35].

When cells were subjected to sound-guided assembly ("A"), a distinct signature of upregulated genes was identified (Group 2). This group includes genes involved in cell organization and signaling. For example, Integrin Subunit Alpha 8 (*ITGA8*) encodes for the α8 subunit of α8β1 integrin, which is responsible for fibronectin binding [36, 37]. From a mechanotransductive perspective, the upregulation of *ITGA8* indicates that cells sense the initial assembly process through integrin-mediated adhesions, which not only contribute to the maintenance of the stem cell population but also influence stem cell proliferation and differentiation [38].

The up-regulation of Transmembrane Protein 64 (*TMEM64*) can be involved in a metabolic shift of the aggregating cells as it is known to act upstream regulation of ATP-dependent activity [39]. On the same

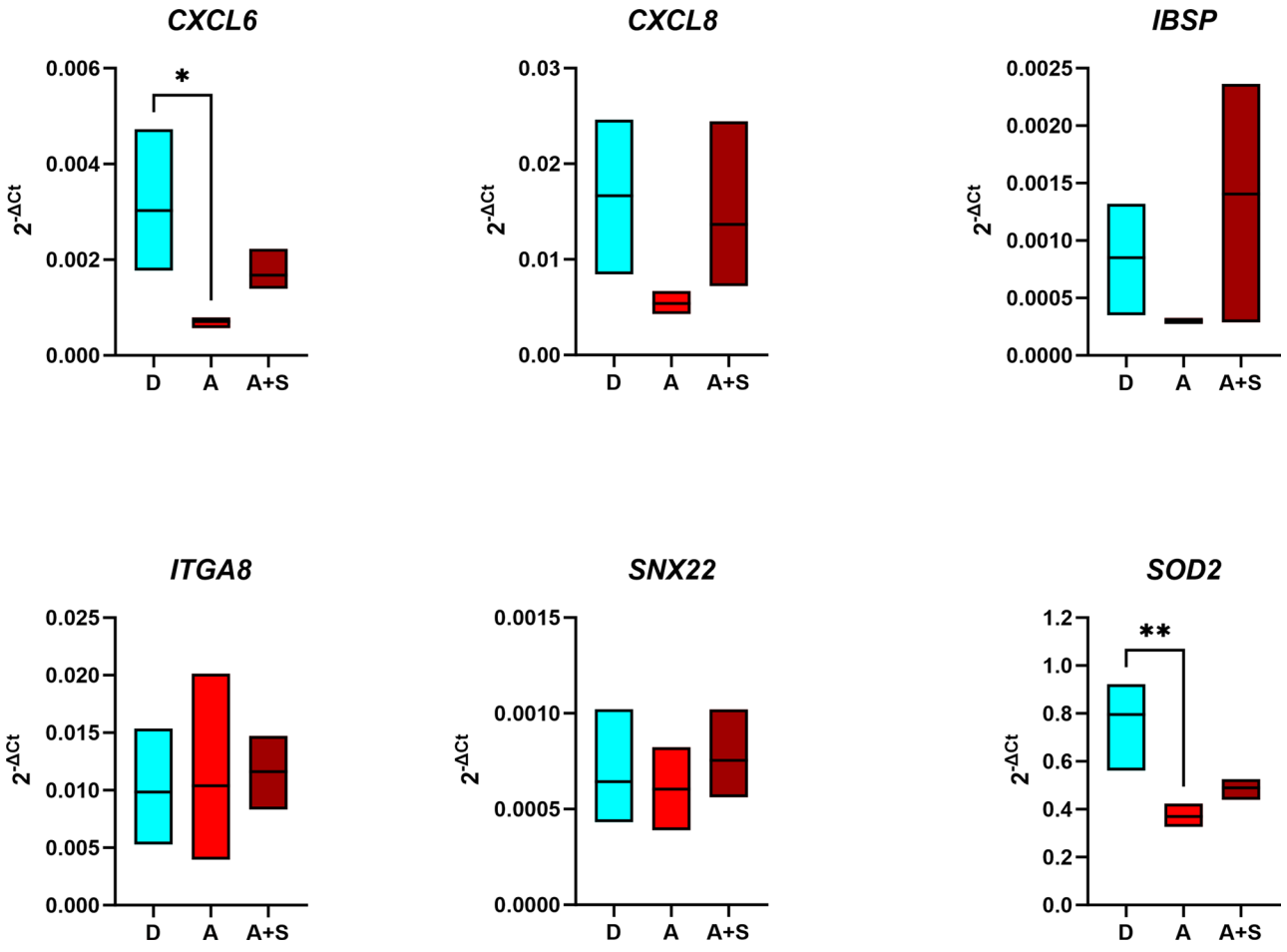


Fig. 3 Gene expression analysis of human mesenchymal stromal cells (hBMSCs) dispersed spheroids (D), after sound-guided assembly (A), and after assembly with further acoustic stimulation (A + S). The relative gene expression levels were analyzed by reverse transcription-quantitative PCR (RT-qPCR) and were calculated by $2^{-\Delta Cq}$ method with normalization to the levels of *GAPDH*. Results are graphically represented as floating bars ranging from min to max, with the line set at the mean $2^{-\Delta Cq}$ value ($n = 3$). Statistical analysis was done with an ordinary one-way ANOVA followed by Dunnett's test to compare D vs. A, and A + S vs. A. * $p < 0.05$; ** $p < 0.01$

direction, the upregulation of Chordin Like 1 (*CHRDL1*) was reported to promote the topographic retinotectal projection in the regulation of retinal angiogenesis [40], further evidence that acoustic stimulation can act as a guidance signal for cells. Interestingly, both *TMEM64* and *CHRDL1* genes are negative regulators of differentiation (antagonists of bone morphogenetic proteins) and positive promoters of proliferation, aggregation and extracellular matrix formation [41, 42]. The presence in Group 2 of snRNAs part of the U1 snRNP complex is coherent with what reported in smooth muscle cells, where this class of snRNAs was upregulated in differentiating vs. proliferating cells [43].

Finally, further acoustic stimulation following sound-guided assembly ("A + S") upregulated the expression of a distinct set of transcripts, that here we report in Group 3. Many of those represent either long noncoding RNAs or other transcripts with unknown functions. Upregulated protein coding genes include some involved in osteogenic differentiation and/or mechanoresponses, such as Integrin Binding Sialoprotein (IBSP) [44], Sorting Nexin 22 (*SNX22*) [45], Matrix Metallopeptidase 13 (*MMP13*) [46], and Desmin (*DES*) [47]. Group 3 protein-coding genes are also involved in matrix formation and maintenance. For example, the Matrix Remodeling Associated 5 (*MXRA5*) gene encodes for an adhesion proteoglycan [48] *DES* upregulation can be important in regulating cell aggregation as it encodes for a specific class of intermediate filaments aimed at forming a stable intracytoplasmic filamentous network connecting myofibrils to each other and to the plasma membrane [49]. It is plausible that the repeated acoustic forces are transmitted through the fibrin matrix to integrin receptors established during the initial assembly. This mechanical signal is subsequently transduced intracellularly, as indicated by the upregulation of the gene encoding for the cytoskeletal protein desmin (*DES*), which contributes to stabilizing the cell's internal architecture. The sustained

mechanotransductive signaling cascade appears to converge on transcription factors that initiate a specific osteogenic program, as evidenced by the expression of *IBSP* and *MMP13*.

The circular pattern generated by the SIM device is biologically significant because it concentrates hBMSC spheroids into a high-density annular region, while maintaining a surrounding zone of lower density. This organization resembles natural condensation phenomena observed during tissue morphogenesis, where local crowding triggers signaling events associated with cell–cell communication, integrin activation, and mechanical feedback. The uniform curvature of the ring geometry also distributes mechanical stress isotropically, minimizing edge effects and promoting balanced radial diffusion of nutrients and paracrine factors. Compared to randomly dispersed spheroids, this spatial confinement likely reduces oxidative and inflammatory signaling while enhancing matrix-related and mechanoresponsive gene expression, as supported by the observed transcriptional changes in *SOD2*, *CXCL6*, *ITGA8*, and *IBSP*. Thus, the donut-like configuration provides a reproducible and biologically relevant microenvironment to study how controlled spatial condensation influences stem cell behavior.

It is worth considering whether the same spatial organization and transcriptional responses could be achieved using alternative, non-acoustic patterning strategies. Methods such as photopatterning [50], scaffolding [51], bioprinting [52], or magnetic assembly [53] can reproduce defined geometries and thus mimic some aspects of spatial confinement. However, these approaches generally rely on surface modification, physical confinement, or external chemical gradients to achieve patterning, introducing additional variables that may independently influence cell behavior. In contrast, sound-guided assembly operates through transient acoustic pressure gradients and hydrodynamic flows that induce rapid, contactless condensation of spheroids without altering the biochemical composition of the surrounding matrix. This process inherently generates dynamic mechanical cues that act synergistically with the imposed geometry, influencing integrin-mediated mechanotransduction and cytoskeletal organization. Therefore, the transcriptional changes observed in this study likely result from the combined effect of spatial condensation and the mechanical microenvironment created by the acoustic field, features that distinguish sound-guided assembly from purely geometrical patterning methods.

The stimulation parameters applied in this study (100 Hz, 1 h/day for 7 days) were chosen based on prior work using the same SIM technology, which demonstrated that low-frequency vibrations (80–120 Hz) can efficiently transmit mechanical cues through soft hydrogels while preserving construct integrity [16, 17]. In our experiments, the 100 Hz condition was selected as a stable and reproducible setting to investigate whether additional mechanical stimulation could influence the transcriptional response of pre-assembled spheroids. Indeed, the RNA-seq data indicated that the A + S group exhibited upregulation of mechanoresponsive and matrix-related genes such as *IBSP*, *MMP13*, *MXRA5*, and *DES*, suggesting that the applied stimulation triggered pathways related to extracellular matrix remodeling and early osteogenic activation. While these results confirm that the selected stimulation parameters were biologically effective without compromising construct geometry, we acknowledge that alternative frequencies, amplitudes, or temporal patterns could lead to different cellular outcomes. Future studies will therefore aim to systematically compare stimulation regimes to delineate the frequency- and dose-dependence of acoustic mechanoactivation in hBMSCs.

Overall, these results underscore the advantage of using SIM technology to enhance local cell density in 3D hydrogel systems without altering the total cell number or matrix composition. By enabling precise spatial arrangement of hBMSC spheroids, SIM creates regions of increased local density, which in turn modulates the microenvironment, affecting the distribution of soluble factors and mechanical cues that are critical for cell behavior. Unlike previous studies that primarily showcased SIM ability for rapid, non-contact cell patterning [16, 17], our current work demonstrates its functional impact: we provide transcriptomic evidence that acoustic patterning and stimulation can actively influence gene expression in hBMSC spheroids. Similarly, we showed before that sound-guided cell patterning drive molecular and functional changes, including protein regulation in vascular cells and spatially guided axonal growth in sensory ganglion models [12, 13]. Furthermore, these data support the delineation of mechanotransductive pathways involved in the observed cellular responses. The transition from condition "D" to "A" underscores the role of cell–matrix sensing, primarily mediated by integrins such as *ITGA8*. The changes in the "A + S" group suggest that continuous acoustic stimulation propagates mechanical signals through the matrix, engages integrin receptors, and transmits forces via the cytoskeleton to the nucleus. This cascade ultimately activates transcriptional programs associated with osteogenesis, as evidenced by the upregulation of *IBSP* and *MMP13*. This positions SIM not just as a structural tool, but as a biologically active method for guiding stem cell responses.

Importantly, this approach offers a non-biochemical strategy to influence cell fate, potentially reducing reliance on growth factors in tissue engineering.

Conclusions

We provide a method for acoustic assembly and stimulation of hBMSC spheroids in fibrin hydrogels, enabling rapid spatial organization and modulation of gene expression. The workflow is compatible with common cell culture practices, adaptable to various cell types, and suitable for mechanistic studies or engineered tissue model development. For the future, we envision that different protocols of acoustic stimulation following sound-guided assembly of cells and spheroids can be optimized and used to drive specific cell responses in terms of differentiation, complementing or substituting the need for growth factors in tissue engineering strategies. Our proof-of-concept results support its use in diverse applications where spatial control and mechanical cues are critical.

Supplementary Information

The online version contains supplementary material available at https://doi.org/10.1186/s44330-026-00070-x.

Supplementary Material 1

Supplementary Material 2

Acknowledgements

We acknowledge the support of the Data Analysis Core Facility (Centro per le malattie autoimmuni e allergiche, Università del Piemonte Orientale – CAAD-UPO) and thank Dr. Francesco Favero for technical assistance.

Author contributions

E.D.B. and A.C. writing the manuscript. E.D.B., F.D., A.C., J.M., R.T. performing experiments and/or analyzing data. M.A., A.Co, M.J.S., L.R., T.S. revising the manuscript. T.S. concept.

Funding

The work was financially supported by AO Foundation and AO CMF (project: AOCMF-21–04 S). AO CMF is a clinical division of the AO Foundation — an independent medically guided not-for-profit organization.

Data availability

Datasets are available from the corresponding author upon reasonable request. RNA sequencing data are deposited on NCBI Gene Expression Omnibus (GEO) with accession number GSE319241 (https://www.ncbi.nlm.nih.gov/geo/query/acc.cgi?acc=GSE319241). RNA sequencing raw and normalized counts are available in Supplementary File 1 and 2, respectively.

Declarations

Ethical approval

The study was conducted in accordance with the Declaration of Helsinki. hBMSCs were previously obtained from a 58-years old male donor, undergoing spinal surgery at the Freiburg University Hospital, Germany, with written informed consent and full ethical approval (Ethik-Kommission der Albert-Ludwigs-Universität Freiburg, EK-326/08).

Consent to participate

Not applicable.

Consent for publication

Not applicable.

Competing interests

The authors declare no competing interests.

Author details

[1]AO Research Institute Davos, Davos Platz, Switzerland
[2]Department of Health Science CAAD, University of Piemonte Orientale UPO, Novara, Italy
[3]Complex Tissue Regeneration Department, MERLN Institute for Technology-Inspired Regenerative Medicine, Maastricht University, Maastricht, Netherlands
[4]Department of Orthopaedics and Trauma Surgery, Medical Centre, Faculty of Medicine, Albert Ludwigs University of Freiburg, Freiburg, Germany

Received: 13 August 2025 / Accepted: 19 February 2026
Published online: 01 May 2026

References

1. Pittenger MF, Mackay AM, Beck SC, et al. Multilineage potential of adult human mesenchymal stem cells. Science Apr 2. 1999;284(5411):143–7. https://doi.org/10.1126/science.284.5411.143.
2. Barry FP, Murphy JM. Mesenchymal stem cells: clinical applications and biological characterization. Int J Biochem Cell Biol Apr. 2004;36(4):568–84. https://doi.org/10.1016/j.biocel.2003.11.001.
3. Engler AJ, Sen S, Sweeney HL, Discher DE. Matrix elasticity directs stem cell lineage specification. Cell Aug. 2006;25(4):677–89. https://doi.org/10.1016/j.cell.2006.06.044.
4. Discher DE, Mooney DJ, Zandstra PW. Growth factors, matrices, and forces combine and control stem cells. Science Jun. 2009;26(5935):1673–7. https://doi.org/10.1126/science.1171643.
5. Mitragotri S. Healing sound: the use of ultrasound in drug delivery and other therapeutic applications. Nat Rev Drug Discov Mar. 2005;4(3):255–60. https://doi.org/10.1038/nrd1662.
6. Xia P, Shi Y, Wang X, Li X. Advances in the application of low-intensity pulsed ultrasound to mesenchymal stem cells. Stem Cell Res Ther. 2022/05/26 2022;13(1):214. https://doi.org/10.1186/s13287-022-02887-z.
7. Yoon JH, Roh EY, Shin S, et al. Introducing pulsed low-intensity ultrasound to culturing human umbilical cord-derived mesenchymal stem cells. Biotechnol Lett Mar. 2009;31(3):329–35. https://doi.org/10.1007/s10529-008-9872-5.
8. Ding X, Lin S-CS, Kiraly B et al. On-chip manipulation of single microparticles, cells, and organisms using surface acoustic waves. Proceedings of the National Academy of Sciences. 2012;109(28):11105–11109. https://doi.org/10.1073/pnas.1209288109.
9. Guo F, Li P, French JB, et al. Controlling cell-cell interactions using surface acoustic waves. Proc Natl Acad Sci U S A Jan. 2015;6(1):43–8. https://doi.org/10.1073/pnas.1422068112.
10. Armstrong JPK, Puetzer JL, Serio A, et al. Engineering Anisotropic Muscle Tissue using Acoustic Cell Patterning. Adv Mater Oct. 2018;30(43):e1802649. https://doi.org/10.1002/adma.201802649.
11. Ozcelik A, Rufo J, Guo F, et al. Acoustic tweezers for the life sciences. Nat Methods Dec. 2018;15(12):1021–8. https://doi.org/10.1038/s41592-018-0222-9.
12. Di Marzio N, Tognato R, Bella ED, et al. Differential proteomics profile of microcapillary networks in response to sound pattern-driven local cell density enhancement. Biomaterials Biosystems. 2024;14:100094. https://doi.org/10.1016/j.bbiosy.2024.100094. 2024/06/01.
13. Ma J, Eglauf J, Grad S, Alini M, Serra T. Engineering Sensory Ganglion Multicellular System to Model Tissue Nerve Ingrowth. Adv Sci (Weinh) Mar. 2024;11(11):e2308478. https://doi.org/10.1002/advs.202308478.
14. Armiento AR, Ladner YD, Della Bella E, Stoddart MJ. Isolation and in vitro chondrogenic differentiation of human bone marrow-derived mesenchymal stromal cells. In: Stoddart MJ, Della Bella E, Armiento AR, eds. Cartilage Tissue Engineering. Springer US; 2023:65–73:chap Chap. 6. Methods in Molecular Biology.
15. Ladner YD, Armiento AR, Kubosch EJ, Snedeker JG, Stoddart MJ. Optimization of loading protocols for tissue engineering experiments. Sci Rep. 2022/03/24 2022;12(1):5094. https://doi.org/10.1038/s41598-022-08849-y.
16. Tognato R, Parolini R, Jahangir S, et al. Sound-based assembly of three-dimensional cellularized and acellularized constructs. Mater Today Bio Oct. 2023;22:100775. https://doi.org/10.1016/j.mtbio.2023.100775.
17. Petta D, Basoli V, Pellicciotta D, et al. Sound-induced morphogenesis of multicellular systems for rapid orchestration of vascular networks. Biofabrication Oct. 2020;16(1). https://doi.org/10.1088/1758-5090/abbb9c.

18. Peng T, Thorn K, Schroeder T, et al. A BaSiC tool for background and shading correction of optical microscopy images. Nat Commun Jun. 2017;8:8:14836. https://doi.org/10.1038/ncomms14836.
19. Daou F, Masante B, Gabetti S, et al. Unraveling the transcriptome profile of pulsed electromagnetic field stimulation in bone regeneration using a bioreactor-based investigation platform. Bone May. 2024;182:117065. https://doi.org/10.1016/j.bone.2024.117065.
20. Andrews S. FastQC: A quality control tool for high throughput sequence data [Online]. http://www.bioinformatics.babraham.ac.uk/projects/fastqc/.
21. Ewels P, Magnusson M, Lundin S, Kaller M. MultiQC: summarize analysis results for multiple tools and samples in a single report. Bioinformatics Oct 1. 2016;32(19):3047–8. https://doi.org/10.1093/bioinformatics/btw354.
22. Li B, Dewey CN. RSEM: accurate transcript quantification from RNA-Seq data with or without a reference genome. BMC Bioinformatics Aug. 2011;4(1):323. https://doi.org/10.1186/1471-2105-12-323.
23. Cunningham F, Allen JE, Allen J, et al. Ensembl 2022. Nucleic Acids Res Jan. 2022;7(D1):D988–95. https://doi.org/10.1093/nar/gkab1049.
24. Dobin A, Davis CA, Schlesinger F, et al. STAR: ultrafast universal RNA-seq aligner. Bioinformatics Jan 1. 2013;29(1):15–21. https://doi.org/10.1093/bioinformatics/bts635.
25. Love MI, Huber W, Anders S. Moderated estimation of fold change and dispersion for RNA-seq data with DESeq2. Genome Biol. 2014;15(12):550. https://doi.org/10.1186/s13059-014-0550-8.
26. Wickham H. *ggplot2*. Use R! New York: Springer-; 2016.
27. Ligorio C, Cianciosi A, Tognato R, et al. Bioconvergence of sound-guided and supramolecular assembly strategies to create peptide-protein composite hydrogels with predictable shape-to-function features. bioRxiv. 2025. 2025.06.26.661668.
28. Wang X, Dai Y, Zhang X, et al. CXCL6 regulates cell permeability, proliferation, and apoptosis after ischemia-reperfusion injury by modulating Sirt3 expression via AKT/FOXO3a activation. Cancer Biol Ther Jan. 2021;2(1):30–9. https://doi.org/10.1080/15384047.2020.1842705.
29. Zhu J, Aja S, Kim EK, et al. Physiological oxygen level is critical for modeling neuronal metabolism in vitro. J Neurosci Res Feb. 2012;90(2):422–34. https://doi.org/10.1002/jnr.22765.
30. Pani G, Colavitti R, Bedogni B, Anzevino R, Borrello S, Galeotti T. A redox signaling mechanism for density-dependent inhibition of cell growth. J Biol Chem Dec. 2000;8(49):38891–9. https://doi.org/10.1074/jbc.M007319200.
31. Pavel M, Renna M, Park SJ, et al. Contact inhibition controls cell survival and proliferation via YAP/TAZ-autophagy axis. Nat Commun Jul. 2018;27(1):2961. https://doi.org/10.1038/s41467-018-05388-x.
32. Miao L, St Clair DK. Regulation of superoxide dismutase genes: implications in disease. Free Radic Biol Med Aug. 2009;15(4):344–56. https://doi.org/10.1016/j.freeradbiomed.2009.05.018.
33. Seghatoleslami MR, Tuan RS. Cell density dependent regulation of AP-1 activity is important for chondrogenic differentiation of C3H10T1/2 mesenchymal cells. J Cell Biochem. 2002;84(2):237–48. https://doi.org/10.1002/jcb.10019.
34. Zaniolo K, Gingras ME, Audette M, Guerin SL. Expression of the gene encoding poly(ADP-ribose) polymerase-1 is modulated by fibronectin during corneal wound healing. Invest Ophthalmol Vis Sci Oct. 2006;47(10):4199–210. https://doi.org/10.1167/iovs.06-0176.
35. Gingras ME, Larouche K, Larouche N, Leclerc S, Salesse C, Guerin SL. Regulation of the integrin subunit alpha5 gene promoter by the transcription factors Sp1/Sp3 is influenced by the cell density in rabbit corneal epithelial cells. Invest Ophthalmol Vis Sci Sep. 2003;44(9):3742–55. https://doi.org/10.1167/iovs.03-0191.
36. Marek I, Lichtneger T, Cordasic N, et al. Alpha8 Integrin (Itga8) Signalling Attenuates Chronic Renal Interstitial Fibrosis by Reducing Fibroblast Activation, Not by Interfering with Regulation of Cell Turnover. PLoS ONE. 2016;11(3):e0150471. https://doi.org/10.1371/journal.pone.0150471.
37. Müller U, Bossy B, Venstrom K, Reichardt LF. Integrin alpha 8 beta 1 promotes attachment, cell spreading, and neurite outgrowth on fibronectin. Mol Biol Cell Apr. 1995;6(4):433–48. https://doi.org/10.1091/mbc.6.4.433.
38. Isomursu A, Lerche M, Taskinen ME, Ivaska J, Peuhu E. Integrin signaling and mechanotransduction in regulation of somatic stem cells. Exp Cell Res. 2019/05/15/ 2019;378(2):217–225. https://doi.org/10.1016/j.yexcr.2019.01.027.
39. Chen GL, Li JY, Chen X, et al. Mechanosensitive channels TMEM63A and TMEM63B mediate lung inflation-induced surfactant secretion. J Clin Invest Dec. 2024;21(5). https://doi.org/10.1172/JCI174508.
40. Webb TR, Matarin M, Gardner JC, et al. X-linked megalocornea caused by mutations in CHRDL1 identifies an essential role for ventroptin in anterior segment development. Am J Hum Genet Feb. 2012;10(2):247–59. https://doi.org/10.1016/j.ajhg.2011.12.019.
41. Liu D, Pu Z, Li B, Tan G, Xie T, Shen Y. Chrdl1-mediated BMP4 inhibition disrupts the balance between retinal neurons and Muller Glia. Cell Death Discov Aug. 2024;17(1):367. https://doi.org/10.1038/s41420-024-02129-6.
42. Kim H, Kim T, Jeong BC, et al. Tmem64 modulates calcium signaling during RANKL-mediated osteoclast differentiation. Cell Metab Feb. 2013;5(2):249–60. https://doi.org/10.1016/j.cmet.2013.01.002.
43. Llorian M, Gooding C, Bellora N, et al. The alternative splicing program of differentiated smooth muscle cells involves concerted non-productive splicing of post-transcriptional regulators. Nucleic Acids Res Oct. 2016;14(18):8933–50. https://doi.org/10.1093/nar/gkw560.
44. Li Y, Ge C, Long JP, et al. Biomechanical stimulation of osteoblast gene expression requires phosphorylation of the RUNX2 transcription factor. J Bone Min Res Jun. 2012;27(6):1263–74. https://doi.org/10.1002/jbmr.1574.
45. Lei H, Sun J, Dai Z, et al. Remote coupling of electrical and mechanical cues by diurnal photothermal irradiation synergistically promotes bone regeneration. J Nanobiotechnology Jul. 2024;11(1):410. https://doi.org/10.1186/s12951-024-02671-6.
46. Tetsunaga T, Nishida K, Furumatsu T, et al. Regulation of mechanical stress-induced MMP-13 and ADAMTS-5 expression by RUNX-2 transcriptional factor in SW1353 chondrocyte-like cells. Osteoarthritis Cartilage Feb. 2011;19(2):222–32. https://doi.org/10.1016/j.joca.2010.11.004.
47. Trumbull A, Subramanian G, Yildirim-Ayan E. Mechanoresponsive musculoskeletal tissue differentiation of adipose-derived stem cells. BioMedical Engineering OnLine. 2016/04/22 2016;15(1):43. https://doi.org/10.1186/s12938-016-0150-9.
48. Walker MG, Volkmuth W. Cell adhesion and matrix remodeling genes identified by co-expression analysis. Gene Funct Dis. 2002;3(3–4):109–12. https://doi.org/10.1002/gnfd.200290000.
49. Sheng JJ, Feng HZ, Pinto JR, Wei H, Jin JP. Increases of desmin and alpha-actinin in mouse cardiac myofibrils as a response to diastolic dysfunction. J Mol Cell Cardiol Oct. 2016;99:218–29. https://doi.org/10.1016/j.yjmcc.2015.10.035.
50. Rana D, Padmanaban P, Becker M, et al. Spatial control of self-organizing vascular networks with programmable aptamer-tethered growth factor photopatterning. Mater Today Bio Apr. 2023;19:100551. https://doi.org/10.1016/j.mtbio.2023.100551.
51. Veenendaal L, Longoni A, Hooper GJ, Lim KS, Woodfield TBF, Lindberg GCJ. 3D-Bioassembly of VH-Spheroids for Cartilage Regeneration: in Vitro Evaluation of Chondrogenesis, Fusion and Lateral Integration. Adv Mater Interfaces. 2022;9(31):2200882. https://doi.org/10.1002/admi.202200882.
52. Roth JG, Brunel LG, Huang MS, et al. Spatially controlled construction of assembloids using bioprinting. Nat Commun. 2023/07/19 2023;14(1):4346. https://doi.org/10.1038/s41467-023-40006-5.
53. Ioannidis K, Dimopoulos A, Decoene I, et al. 4D Biofabrication of Magnetically Augmented Callus Assembloid Implants Enables Rapid Endochondral Ossification via Activation of Mechanosensitive Pathways. Adv Sci. 2025;12(15):2413680. https://doi.org/10.1002/advs.202413680.

Publisher's note

Springer Nature remains neutral with regard to jurisdictional claims in published maps and institutional affiliations.